

DIRECT 3D PATTERN MATCHING IN THE DOMAIN OF FREEFORM SHAPES

Joris S.M. Vergeest, Sander Spanjaard, Yu Song

Faculty of Design, Engineering and Production
Delft University of Technology, Jaffalaan 9
NL-2628 BX Delft
The Netherlands

j.s.m.vergeest@io.tudelft.nl

<http://dutoa36.io.tudelft.nl>

ABSTRACT

We have studied the problem of extracting shape parameters from freeform features in full 3D. The freeform features are typically encountered in laser-scanned data from physical parts or in point clouds from any source. Matching involves 1) the search for optimal position and orientation of the template shape and 2) the adjustment of a number (d) of intrinsic shape parameters. The type and total number of parameters ($6+d$), and hence the family of template shapes is determined by the type of feature. We have analyzed the robustness, accuracy and the efficiency of Hausdorff-like shape distance measures. A number of search strategies have been tested and were evaluated against convergence and computational performance. The practical relevance of the technique is addressed as well.

Keywords: freeform shape, freeform features, point cloud, shape matching, Hausdorff distance, optimization,

1. INTRODUCTION

Object recognition and shape matching are relatively new techniques. Most of literature on shape (or shape feature) recognition is in the domain of images, or based on 2D geometric projections or silhouettes from higher-dimensional objects. In some applications, however, the representation and processing of the geometric objects themselves, in full 3D, is demanded. These applications include object surface analysis, geometric inspection, surface reconstruction and reverse engineering of shape. Typically, a match is sought between a measured (digitized) object and an already available model, either in some library or generated synthetically.

In this paper we propose a method for the direct, partial matching of 3D surfaces. Direct, here, refers to the calculation of the matching criterion explicitly from the surface points, using the Hausdorff distance, defined later. Partial means that it is sufficient that one of the shapes matches to only some portion of the other shape. The motivation for this approach stems from the application that we support, namely the reuse of (portions of) existing

shapes as shape features in a new Computer-Aided Design (CAD) model. This made it necessary that the matching depends not only on an affine transformation, but on intrinsic shape parameters as well. Before going into detail of the matching technique and of the driving application, we will briefly mention some of the existing 3D shape matching methods. For a more elaborate overview we refer to [Barequet 1997] and [Veltkamp 2001].

Shape matching depends on two functions, the calculation of shape dissimilarity and the search in some space to maximize shape similarity.

For some applications the main task is to search among a large set of predefined, discrete shapes B_i for the one(s) that resemble a given shape A . An example of such an application is the search for a fingerprint in a database. To perform this function some kind of indexing scheme can be introduced, based on global moments, Fourier descriptors, local geometric properties or even strain energy [Prokop 1992], [S. Loncaric 1998], [Sclaroff 1995]. If it is known beforehand that the set $\{B_i\}$ consists of shapes exhibiting particular features or singularities, then an indexing scheme can be based on the type

and/or number of such features in each of the members B_i .

For the purpose of quality control a manufactured part B can be compared against the CAD model A it originated from. First the surface of the manufactured part is digitized and the point set is tested for matching the (surface or solid) model A . This involves a search among a continuous set of shapes $P(B)$, where P denotes translations and rotations and possibly scaling as well, leading to a 6- or 7-dimensional search space. When the best alignment of $P(B)$ with A is achieved, the positional deviation between the two shapes can be analysed and visualized. For this purpose, commercial software systems are readily available [Mieritz 1999].

Reverse engineering of a 3D part B comprises the reconstruction of a CAD model from measured points on B . If the CAD model is hypothesized to consist of known types of surfaces A_i (e.g. cylinders and planar sections) the surfaces A_i must be matched to (portions of) B [Tangelder 1999], [Thompson 1999]. If the CAD model is of a more generic type A , for example represented as a set of NURBS surfaces, then the task of reverse engineering is reduced to the reconstruction of A from data B , without explicit shape matching [Váradi 1997].

Although the applications listed above are in three dimensions, most of the published work on shape recognition and matching deals with applications and with algorithms tested in 2D, as e.g. in [Kwon 2001]. Many search strategies for 3D applications are based on 2D derivations from the models to be matched, as for example in [Johnson 1998], [Li 2000].

As mentioned, search strategies should be distinguished from the actual similarity measure. The complexity of the similarity computation depends on the requirements from the application. If it is needed to select from a set $\{B_i\}$ the shape which is most similar (but perhaps far from congruent) to A then it may be sufficient to use a low-cost similarity measure. On the other extreme, if a best fit between shape A and a shape B from a continuously varying set of shapes, then the similarity computation will normally be complex. This is especially true for freeform shapes, properties of which can sometimes be numerically approximated only.

2. APPLICATION IN GEOMETRIC MODELING

The requirements on both the similarity computation and on the search strategy derive from the intended application. We have developed an approximation of the directed Hausdorff distance between 3D shapes, defined in the next section. Here we explain this

choice. The shapes of interest are portions of the boundaries of 3D solids, hence the shapes can be considered as 2-manifolds. When a 3D solid or surface CAD model is developed it is, in some situations, effective that the designer reuses an existing shape. In doing so, the designer may save considerable time and effort. However, typically it is not sufficient to perform merely a copy-and-paste action, but the copied shape should be adapted to the target model. This adaptation can be partly automatic (e.g. to achieve geometric continuity between copied shape and the target shape) and should be partly controlled by the user (e.g. by modifying particular shape parameters). More detailed information about methodological issues of the shape reuse process can be found in [Vergeest 2001a]. The application comprises four basic steps:

1. A geometric representation S of the shape to be reused must be obtained. This involves either the digitization of a (portion of a) physical object or the selection of (a portion of) a shape which was already in digital form. In the latter case the shape may originate from the user's local files, or from a company's shape library, or it may be found on the internet.
2. The representation S obtained in step 1 should be modeled as a parameterizable shape $T(p)$, where those parameters p should be available to the user that he/she will need later to adjust the shape before its insertion into the target model. This involves the matching of shapes $T(p)$ to shape S . Matching is the minimization of $D(T(p), S)$, where D is a nonnegative scalar function of a pair of shapes. It should be noted that the multi-dimensional parameter p always includes the 6 DOF for rigid body transformation.
3. The user adjusts the parameter p to the value $p = p'$ to obtain the shape $T(p')$ meeting the current design requirements.
4. Shape $T(p')$ is copied and inserted into the target CAD model.

In step 2 of the application process the actual shape comparison takes place. D needs to be a directed, or partial, shape distance, since in general it is demanded that $T(p)$ matches to a part of S , rather than to S itself.

D needs to be sensitive to small changes of p , where the variations include translation, rotation and intrinsic shape variations of $T(p)$.

For efficiency reasons D should be based on a pre-computation of approximations of S and $T(p)$, where it should be taken into account that shapes $T(p)$ remain congruent under variation of any of the 6 rigid body transformation parameters. Also, portions

of $T(p)$ may be unaffected within certain regions of parameter space.

From these requirements we decided to implement the directed Hausdorff distance from $T(p)$ to S , where the shapes are approximated using discrete points on the shapes.

3. DEFINITIONS

In the following we assume that \mathbb{R}^3 is the ambient space of our application. However, most of the results can be generalized to \mathbb{R}^n , for any $n > 0$.

$S \subset \mathbb{R}^3$ is a portion of the boundary of a compact subset of \mathbb{R}^3 . Without losing generality we assume that S is a 2-manifold in \mathbb{R}^3 . Further, we assume that S is topologically equivalent to a sphere in case S covers the entire boundary of the compact subset; S is topologically equivalent to a square, otherwise. Likewise, $T(p)$ is a 2-manifold in \mathbb{R}^3 and $p \in P$ is called a parameter value from the parameter domain P , which can be any set. Informally, S and $T(p)$ are called 3D shapes. The mapping $T : P \rightarrow 2^{\mathbb{R}^3}$, where $2^{\mathbb{R}^3}$ denotes the power set (the set of subsets) of \mathbb{R}^3 , determines a family of shapes $\{T(p) \in 2^{\mathbb{R}^3} \mid p \in P\}$. T is sometimes called a shape feature type, or a shape template or shape class.

The *Hausdorff distance* $D(T(p), S)$ between the shapes $T(p)$ and S is

$$D(T(p), S) = \max (H(T(p), S), H(S, T(p))),$$

where $H(T(p), S)$ is the *directed Hausdorff distance* from $T(p)$ to S defined as

$$H(T(p), S) = \sup_{t \in T(p)} (\inf_{s \in S} |t - s|), \quad (1)$$

where $|t - s|$ denotes the Euclidean distance between the points s and t . The directed Hausdorff distance $D(S, T(p))$ is defined similarly.

The *mean directed Hausdorff distance* $M(T(p), S)$ is

$$M(T(p), S) = \frac{1}{\text{Area}(T(p))} \iint_{T(p)} \inf_{s \in S} |t - s| dA, \quad (2)$$

where the integration is over the surface of $T(p)$, normalized by the surface area of $T(p)$. The mean directed Hausdorff distance is sometimes preferred over the directed Hausdorff distance, as the latter is sensitive to noise and inaccuracies in the shape data. Indeed, $H(T(p), S)$ is a worst case selection, of the point on $T(p)$ which is farthest from S , whereas $M(T(p), S)$ averages over the distances.

It should be noted that the distances defined in (1) and (2) not only exist for 2-manifolds but for almost any pair of subsets of \mathbb{R}^3 .

4. APPROXIMATION AND COMPUTATION

For special cases, *e.g.* when the shapes $T(p)$ and S are represented in implicit form, equation (1) or (2) or both can be evaluated analytically in closed form. However, in practice this is seldom the case and we need to base the computation on approximations of the shape.

Typically, $T(p)$ is an instance derived from a geometric feature class or, more generally, $T(p)$ is a 2-manifold in some geometric representation form. In the domain of freeform shapes the most common representation forms are surfaces (including B-spline surfaces) or triangulations or surface meshes. As mentioned, $T(p)$ may or may not enclose a volume.

S may be obtained from a measurement and hence be represented by a set of points. S can also originate from a CAD system and hence be available in a geometric representation form.

We decided to base the dissimilarity computation on the point sets $\{t_i \in T(p), i=1, m\}$ and $\{s_j \in S, j=1, n\}$, for some m and n . The points t_i are obtained in two steps. For given $p \in P$ the surface $T(p)$ is computed. Then m points t_i in the surface $T(p)$ are calculated using some sampling strategy. In practice the points s_j are directly available from the 3D object scanner, or they are generated by synthetic sampling if S is a geometric model.

The distances in equations (1) and (2) are then approximated by

$$H(T(p), S) = \max_{i=1, m} (\min_{j=1, n} |t_i - s_j|) \quad (3)$$

and

$$M(T(p), S) = \frac{1}{m} \sum_{i=1, m} (\min_{j=1, n} |t_i - s_j|), \quad (4)$$

respectively, where t_i and s_j are the points in $T(p)$ and S , respectively.

In step 2 described in section 2, a matching procedure is required to obtain the best fitting template $T(p)$ under variation of the parameters p . This involves the search for $p_{opt} \in P$ defined as

$$P_{opt} = \text{Arg} \min_{p \in P} H(T(p), S) \quad (5)$$

or

$$P_{opt} = \text{Arg} \min_{p \in P} M(T(p), S) \quad (6)$$

depending on whether we apply the directed Hausdorff distance or the mean directed Hausdorff distance.

5. COMPUTATION OF SHAPE DISSIMILARITY

In this section we investigate the computation of the directed Hausdorff distance for some concrete shapes. We are particularly interested in the quantitative behavior of $H(T(p),S)$ and $M(T(p),S)$ as a function of p , since this behavior will determine the feasibility of the matching procedure needed in step 2 of Section 2.

5.1 Digitization of object S

The investigated shapes were relevant in a practical case to accomplish a copy-adjust-and-paste action, where the type of feature to be copied was a ridge, see test object A shown in Fig. 1.



Fig. 1. Test object A was digitized to generate the data points s_i . The feature of interest in this object is formed by the longitudinal ridges in the upper surface. The white ellipse indicates the region containing the data representing the shape S .

The length of A is approximately 130 mm and the width of the ridge is approximately 2.5 mm. Two different scanning techniques were used to sample the object. Both scanners are small and fit on a desktop. The first is a mechanical coordinate measuring machine, the Roland PIX-3. The object is placed on a table movable in the horizontal plane, and a vertical needle is a touch trigger probe. Once the object is fixed, the height of the object's surface is measured as a function of the position in the plane. The workspace of the scanner is 150×100×40 mm. The step size of the probe is 0.05 mm minimally. The second device is a desktop laser scanner, the L2000 from Conrad Electronics. A laser beam is projected onto the object, at a series of angles in the vertical plane. Two CCD cameras deliver the data for the determination of the 3D coordinates of the light spots. The object is scanned along multiple vertical lines by way of stepping the platform about the vertical axis.

The surface of the part has been scanned using both of the two devices under a number of different settings of the resolution parameters. Different part orientations were experimented [Broere 2000]. For the investigation in this paper we have used 0.5mm steps of the mechanical scanner and obtained a sample of 24,382 points. With the laser scanner we obtained 360 scan lines containing 61 points each (21,960 points). The difference in scanning time is noticeable, 7.5 hours for the mechanical scanner and only 19 minutes for the laser scanner.. One of the point clouds obtained is shown in Fig. 2. From the point clouds, subsets $\{s_i\}$ can be selected to represent S .

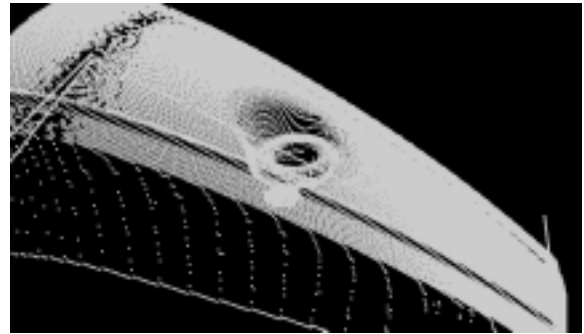


Fig. 2. Point cloud obtained with the mechanical coordinate measuring machine.

5.2 The shape template $T(p)$

We have searched for a partial match of a simple template $T(p)$ of a ridge to the data S . Initially we parameterized the pattern $T(p)$ by 15 parameters as follows (see Fig. 3).

- The coordinates of the points \mathbf{c}_2 and \mathbf{c}_3 in a local coordinate system, with \mathbf{c}_1 at its origin (6 parameters).
- The total width a of the template, the width w and height h of the ridge (3 parameters).
- The orientation of the pattern in a global coordinate system (3 parameters, not shown).
- The location of the template in the global coordinate system is defined by \mathbf{c}_1 , which serves as reference point (3 parameters).

The ridge can also be regarded as a swept profile along a smooth trajectory curve interpolating the three points \mathbf{c}_1 , \mathbf{c}_2 and \mathbf{c}_3 . More complex parameterizations of a ridge pattern are certainly possible. For the numerical tests we kept the three points \mathbf{c}_1 , \mathbf{c}_2 and \mathbf{c}_3 collinear and fixed relative to each other. Also the total width a of $T(p)$ was fixed. Hence, 8 parameters (the 2 profile parameters h and w , and the 6 DoF for the pose) were left effective. Consequently, p is an 8-component vector, $p \in P =$

$\mathbb{R}^3 \times \text{SO}(3) \times \mathbb{R}^2$, the space of rigid body transformations Cartesian-times a two-dimensional space of intrinsic shape deformations.

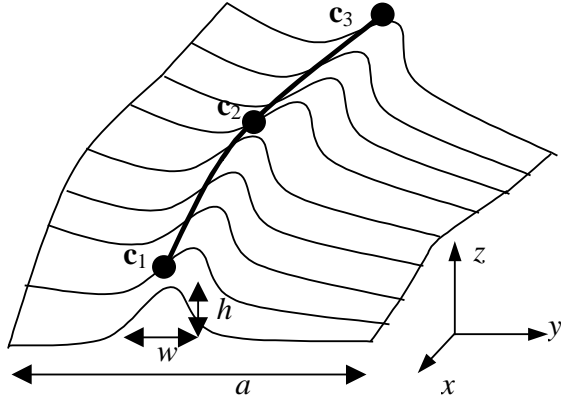


Fig. 3. Parameters for the pattern $T(p)$.

As mentioned, the pattern $T(p)$ needs to be converted into points t_i . This is accomplished by an intermediate NURBS representation of $T(p)$. The intrinsic shape parameters h and w define 11 B-spline control points in the plane; the template $T(p)$ is generated as the NURBS surface defined by 20 such rows of control points in equidistant planes perpendicular to the x -axis. Finally, a user-defined number m of points in the surface constitute the set $\{t_i, 0 < i \leq m\}$. The effect of the parameters h and w on the shape of $T(p)$ is depicted in Fig. 4.

5.3 Sensitivity analysis

One goal of the analysis is a comparison of the behaviors of the distances in (3) and (4). The effect of the difference between the two scanning devices is of interest as well, but is not further considered in this article. It can be expected that near $p = p_{opt}$ as defined in (5) and (6), any deviation of any of p 's components from p_{opt} will cause an increase of the dissimilarity between $T(p)$ and S .

We computed the dissimilarities between the sets $T(p)$ and S represented by the points $\{t_j, j=1, n\}$ and $\{s_i, i=1, m\}$, respectively. A portion of the points scanned on object A (only those within the region indicated in Fig. 1) were actually used for the numerical experiments, $m=2308$ from the points obtained with the mechanical scanner and $m=2261$ from the points obtained with the laser scanner. $n=1300$ points were generated on $T(p)$. A typical configuration of the point sets is depicted in Fig. 5.

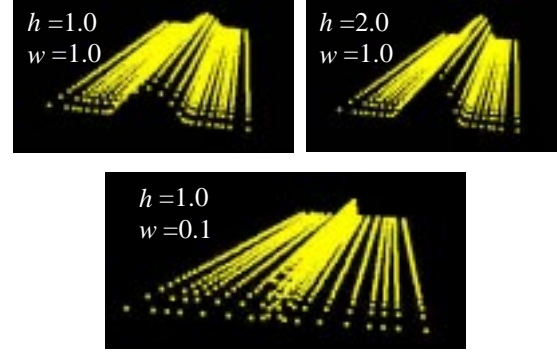


Fig. 4. The ridge template is represented by points on $T(p)$. Variations of $T(p)$ are shown for different values of the intrinsic shape parameters h and w .

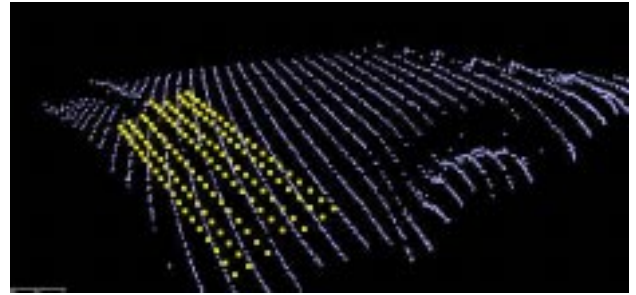


Fig. 5. A portion of the scanned data from object A was used to represent S . The points on the template $T(p)$ are also shown.

Near p_{opt} we expect to observe the ridge structure in both $H(T(p), S)$ and $M(T(p), S)$ as a function of (x, y) ; fig. 6 presents the results.

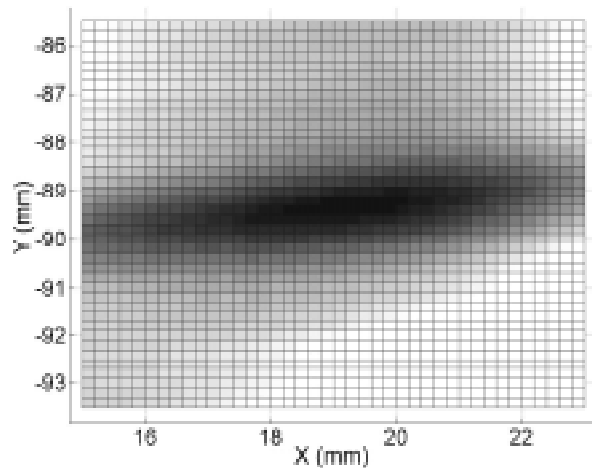


Fig. 6. Hausdorff dissimilarities near p_{opt} as a function of (x, y) . The darkness is proportional to $-M(T(p), S)$.

In Fig. 7 $H(T(p), S)$ and $M(T(p), S)$ are plotted as a function of h and w . We note that by definition $M(S, T(p)) \leq H(T(p), S)$ for all $p \in P$. The plots are obtained near $p = p_{opt}$ with all variables fixed except h and w , respectively. In these cases we may denote $T(p)$ by $T(h)$ and $T(w)$, respectively. It can be seen

that the directed Hausdorff distance is, for the particular data sets, not an appropriate measure to search for the best matching width and height of the template ridge. The quantity $H(T(w),S)$ is flat as a function of w near w_{opt} , the w -component of p_{opt} . However, the mean directed Hausdorff distance $M(T(p),S)$ exhibit a minimum both in h and in w . The estimated values for the intrinsic parameters from fits to the data (see section 6) were $h=2.1$ mm and $w=2.7$ mm.

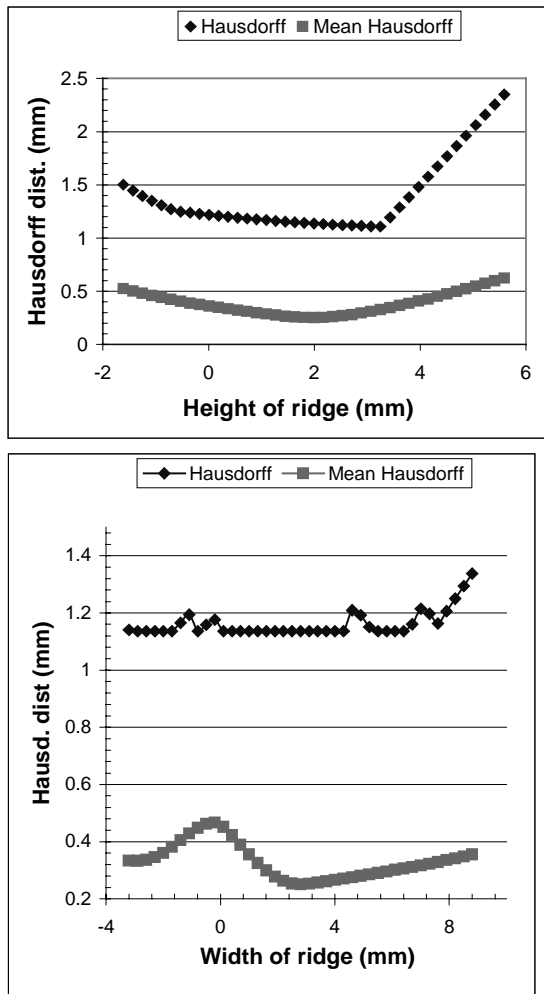


Fig. 7. Top: The dissimilarities $H(T(p),S)$ and $M(T(p),S)$ as a function of the h -component of p . Bottom: The same two quantities as a function of the w -component of p .

6. SEARCH STRATEGIES

One purpose of the distance measure was to determine p_{opt} numerically. The search problem stated in (6) was approached by applying four different fitting strategies [Spanjaard 2001]. In all runs the mean directed Hausdorff distance $M(T(p),S)$ was used on data from the mechanical coordinate measuring machine. In all search strategies the amount of data entering the computation was progressively increased during subsequent stages of the process.

6.1 Overview of different fitting strategies

The fitting strategies differ in the fraction of the points that actually enter the fit, in the number of stages in which the total procedure is divided, and the grouping of different parameters that are fitted concurrently. One semi-automatic and three fully automated fitting strategies were designed, partly based on some heuristics.

In strategy A the fit process consists of two stages. In both stages all 8 parameters are fitted concurrently. To speed up the total fitting time, the percentage of available points is reduced in stage 1

In strategy B, the fit process is divided in five stages. The first two stages should position the template in the neighborhood of the source point set. Stage 3 adjust the ridge's width and height. The two final stages fine tune the fit, where the assumption is made that the minimizer already has aligned the template correctly to the source.

The fit process in strategy C consists of three stages. In the first two stages the translation and orientation parameters are fitted. In the final stage all parameters are fitted simultaneously. During the fit the number of points m is increased from 1% to 100% of the available points in $T(p)$.

Strategy D is a user controlled fit process. The user may suspend the fitting process at any time and roughly force the template toward the correct position and orientation by altering the parameter values manually, either by interactive dragging the template, or by typing parameter values. The fine tune fitting is done by the minimizer.

To prevent extreme long fitting times each stage in a fit has a timeout value. This timeout forces the process to go to the next stage in case the minimizer cannot terminate within a particular amount of time.

6.2 Numerical comparison

The computation was implemented in the Visual C++ programming language from Microsoft on the Windows NT operating system. The Open Inventor package from TGS Inc. was used for visualization and for some basic geometric operations, such as the generation of points on the NURBS surface. The IMSL package from Visual Numerics, Inc. contains a general purpose routine for multivariable scalar function minimization. This routine was used to search for maximal similarity of $T(p)$ to S . Details about the implementation can be found in [Spanjaard 2000].

In Fig. 8 the mean directed Hausdorff distance as function of time is displayed for each of the four fitting strategies.

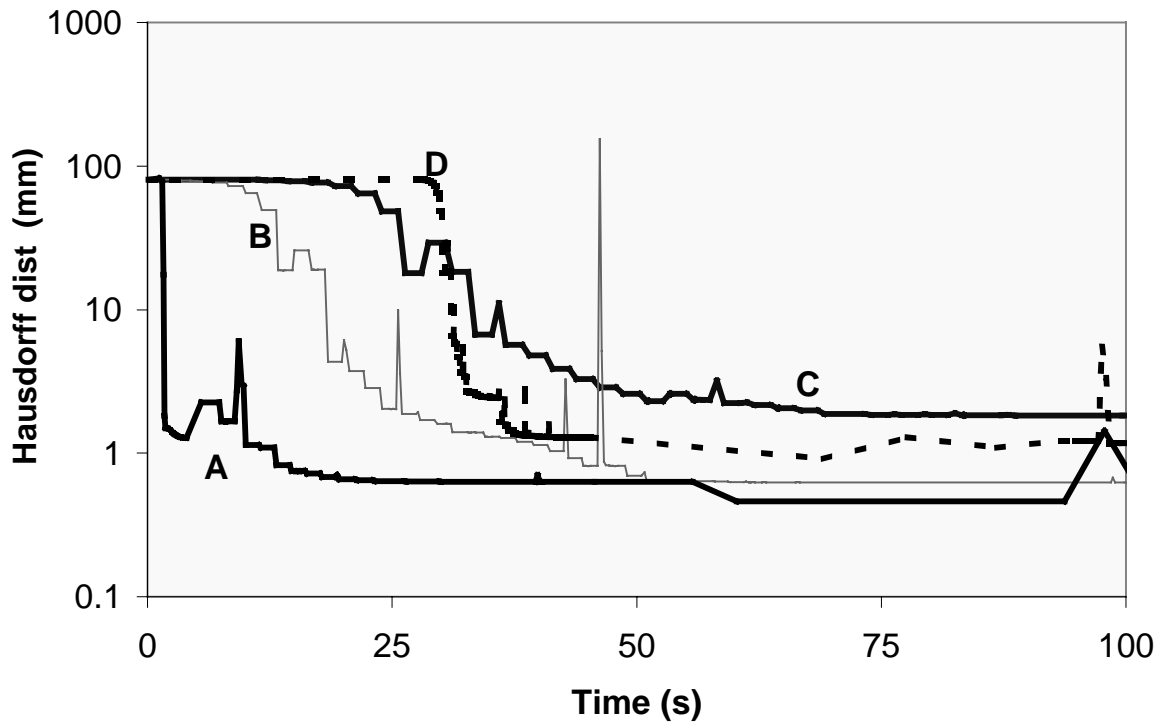


Fig. 8. The first 100 seconds of the mean directed Hausdorff dissimilarity $M(T(p), S)$ as function of elapsed time for fitting strategies A, B, C and D.

Strategy C brings the template to the source fastest. This is because in the first stage of strategy C only 1% of the points are used. Strategies A and D take the longest time to complete. Strategy B is completed after about 460 s. Strategy C, the fastest after about 290 s.

6.3 Discussion

In all four strategies the fits have managed to find the source object in the 3D space. That is they moved the template into the neighborhood of the source. Strategies B and C were also able to orientate the template into the correct plane.

Strategies B and C were able to find the correct plane orientation. However, for both strategies the minimizer was not able to rotate the template in this plane in order to align it with the ridge. The minimizer responded to this problem by making the height parameter almost zero, resulting in the template shape to become a flat surface.

The main problem encountered with fully automated fitting is that the minimizer got trapped at a local minimum.

The best result was achieved with a minor user involvement, in strategy D

7. PERFORMANCE ISSUES

Efficiency is an important issue, considering the optional user involvement during the fitting process.

As mentioned, the reduction of the number of data points during the initial stages of the fits already accelerated the computation considerably, at the cost, however, of accuracy. This inaccuracy can be acceptable, as it speeds up the finding of a near-optimum of $M(T(p), S)$.

Without losing accuracy, the computation was accelerated by applying space binning. A bounding box of S is subdivided in cubes, and points s_j are indexed by the cube they are contained in. In search for

$$\min_{j=1, n} |t_i - s_j|$$

(see (4)), it is then sufficient to consider only the points in cubes nearby t_i . Space binning yielded a reduction of the computation time of up to a factor 20 for large point clouds. A more general reduction of the algorithmic complexity from $O(mn)$ to $O(m \ln n)$ would be obtained by implementing an octree representation of the points $\{s_i, i=1, m\}$. We did however not test this option.

Typically, a minimization process consists of relatively many evaluations of the cost function in which the variation between subsequent points p is small. When $M(T(p), S)$ and $M(T(p+\Delta p), S)$ need to be determined in succession, then much of the computation can be reused for small Δp . This option has not been tested yet

8. CONCLUSIONS AND FURTHER RESEARCH

We have presented the definition and an implementation form of two shape dissimilarity measures in full 3D, the directed Hausdorff distance and the mean directed Hausdorff distance. For noisy and incomplete data samples, the mean directed Hausdorff distance was the preferred measure. Analysis of the shape distance as functions of the parameter components revealed that robust shape matching was feasible. From numerical tests we conclude that such shape features as a ridge in surface could be recognized in data samples. Matching of a synthetic ridge template to the data yielded pose parameters as well as the values for the intrinsic parameters height and width of the ridge.

The ultimate application of the fitting procedure is to support the interactive copy-and-paste of physical shape features into a new CAD model. The most important task of the minimizer is to determine the intrinsic shape parameters of the surface feature. We have shown that this part of the computation was feasible. Current research is directed towards further reduction of the computational complexity of the shape matching. The extension to different types of shape templates, such as a freeform hole in a freeform surface [Vergeest 2001b] is under investigation..

REFERENCES

- [Barequet 1997] G. Barequet and M. Sharir, "Partial surface and volume matching in three dimensions", *IEEE Transactions on Pattern Analysis and Machine Intelligence*, Vol. 19, No. 9, 1997, pp. 1-21.
- [Broere 2000] Broere, "Feature recognition from 3-D model scanning". Technical report, Faculty of Design, Engineering and Production, Delft University of Technology, Delft, 2000.
- [Johnson 1998] A.E. Johnson and M. Hebert, "Surface matching for object recognition in complex three-dimensional scenes", *Image and Vision Computing*, Vol. 16, 1998, pp. 635-651.
- [Kwon 2001] O.-K. Kwon, D.-G. Sim and R.-H. Park, "Robust Hausdorff distance matching algorithms using pyramidal structures", *Pattern Recognition*, Vol. 34, 2001, pp 2005-2013.
- [Loncaric 1998] S. Loncaric, "A survey of shape analysis techniques", *Pattern Recognition*, Vol. 3, No. 8, 1998, pp. 983-1001.
- [Li 2000] C.L. Li and K.C. Hui, "Feature recognition by template matching", *Computers & Graphics*, Vol. 24, 2000, pp. 569-582.
- [Meiritz 1999] B. Meiritz (Ed.), *Conference on Reverse Engineering, 3D scanning and a shortcut to modelling*. Danish Technological Institute, Aarhus, 1999.
- [Prokop 1992] R.J. Prokop and A.P. Reeves, "A survey of moment-based techniques for unoccluded object representation and recognition", *CVGIP: Graphics Models and Image Processing*, Vol. 54, No. 5, 1992, pp. 438-460.
- [Sclaroff 1995] S. Sclaroff and A.P. Pentland, "Modal matching for correspondence and recognition", *IEEE Trans. on Pattern Analysis and Machine Intelligence*, Vol. 17, No. 6, 1995, pp. 545-561.
- [Spanjaard 2000] S. Spanjaard, "Documentation of ridge fit application and its source code". Technical report, Faculty of Design, Engineering and Production, Delft University of Technology, Delft, 2000.
- [Spanjaard 2001] S. Spanjaard and J.S.M. Vergeest, "Comparing different fitting strategies for matching two 3D point sets using a multivariable minimizer" *Proc. of the 2001 Computers and Information in Engineering Conference, DETC'01/CIE-21242*, ASME, New York, 2001.
- [Tangelder 1999] J.W.H. Tangelder, P. Ermes, G. Vosselman, F.A. van den Heuvel, "Measurements of curved objects using gradient based fitting and CSG models", in *International Archives of Photogrammetry and Remote Sensing*, Vol. 32, Part 5W11, 1999, pp. 23-30.
- [Thompson 1999] W.B. Thompson, J.C. Owen, H. James de St. Germain, S.R. Stark and T.C. Henderson, "Feature-based reverse engineering of mechanical parts", *IEEE Tran. Robotics and Automation*, Vol. 15, No 1, 1999, pp. 57-66.
- [Váradi 1997] T. Váradi, R.R. Martin and J. Cox, "Reverse engineering of geometric models - an introduction", *Computer-Aided Design*, Vol. 29, No. 4, 1997, pp. 255-268.
- [Veltkamp 2001] R.C. Veltkamp, "Shape matching: similarity measures and algorithms", *Proc. Shape Modeling International Conference*, a. Pasko and M. Spagnuolo, Eds., Los Alamitos, IEEE, 2001, pp. 188-197.
- [Vergeest 2001a] J.S.M. Vergeest, I. Horváth, S. Spanjaard, "A methodology for reusing freeform shape content", *Proc. of the 2001 Design Theory and Methodology Conference, DETC'01/DTM-21708*, ASME, New York, 2001, CD-ROM proceedings.
- [Vergeest 2001b] J.S.M. Vergeest I. Horváth and S. Spanjaard, "Parameterization of freeform features", In: A. Pasko and M. Spagnuolo (Eds.), *Proc. Shape Modeling International, IMA-CNR, IEEE, Piscataway*, 2001, pp. 20-29.